Supplementary Information for:

Assessment of the global coherence of different types of droughts in model simulations under a high anthropogenic emission scenario

Luis Gimeno-Sotelo[1,2], Ahmed El Kenawy[3], Magí Franquesa[3], Iván Noguera[3], Beatriz Fernández-Duque[3], Fernando Domínguez-Castro[3], Dhais Peña-Angulo[4], Fergus Reig[3], Rogert Sorí[1,2], Luis Gimeno[1,2], Raquel Nieto[1,2], Sergio M. Vicente-Serrano[2,3]

[1]Centro de Investigación Mariña, Universidade de Vigo, Environmental Physics Laboratory (EPhysLab), Ourense, Spain, [2]Unidad Asociada CSIC-Universidad de Vigo: Grupo de Física de la Atmósfera y del Océano, Ourense, Spain,[3]Instituto Pirenaico de Ecología, Consejo Superior de Investigaciones Científicas (IPE–CSIC), Zaragoza, Spain,[4]Department of Geography, University of Zaragoza, Zaragoza,Spain

Tables

Table 1: *CMIP6 models used in this study*

MODEL NAME	**INSTITUTION**	**NATIVE SPATIAL RESOLUTION** (lon x lat)
ACCESS-CM2	CSIRO-ARCCSS	1.875° x 1.25°
ACCESS-ESM1-5	CSIRO	1.875° x 1.25°
CanESM5-CanOE	CCCma	2.8125° x 2.767272°
CanESM5	CCCma	2.8125° x 2.767272°
CMCC-ESM2	CMCC	1.25° x 0.9424084°
CNRM-CM6-1-HR	CNRM-CERFACS	0.5° x 0.49512°
CNRM-CM6-1	CNRM-CERFACS	1.40625° x 1.38903°
CNRM-ESM2-1	CNRM-CERFACS	1.40625° x 1.38903°
FIO-ESM-2-0	FIO-QLNM	1.25° x 0.9424084°
GFDL-ESM4	NOAA-GFDL	1.25° x 1°
GISS-E2-1-G	NASA-GISS	2.5° x 2°
HadGEM3-GC31-LL	MOHC	1.875° x 1.25°
HadGEM3-GC31-MM	MOHC	0.8333333° x 0.5555556°
INM-CM4-8	INM	2° x 1.5°

IPSL-CM6A-LR	IPSL	2.5° x 1.267606°
MIROC-ES2L	MIROC	2.8125° x 2.767272°
MIROC6	MIROC	1.40625° x 1.38903°
MRI-ESM2-0	MRI	1.125° x 1.11209°

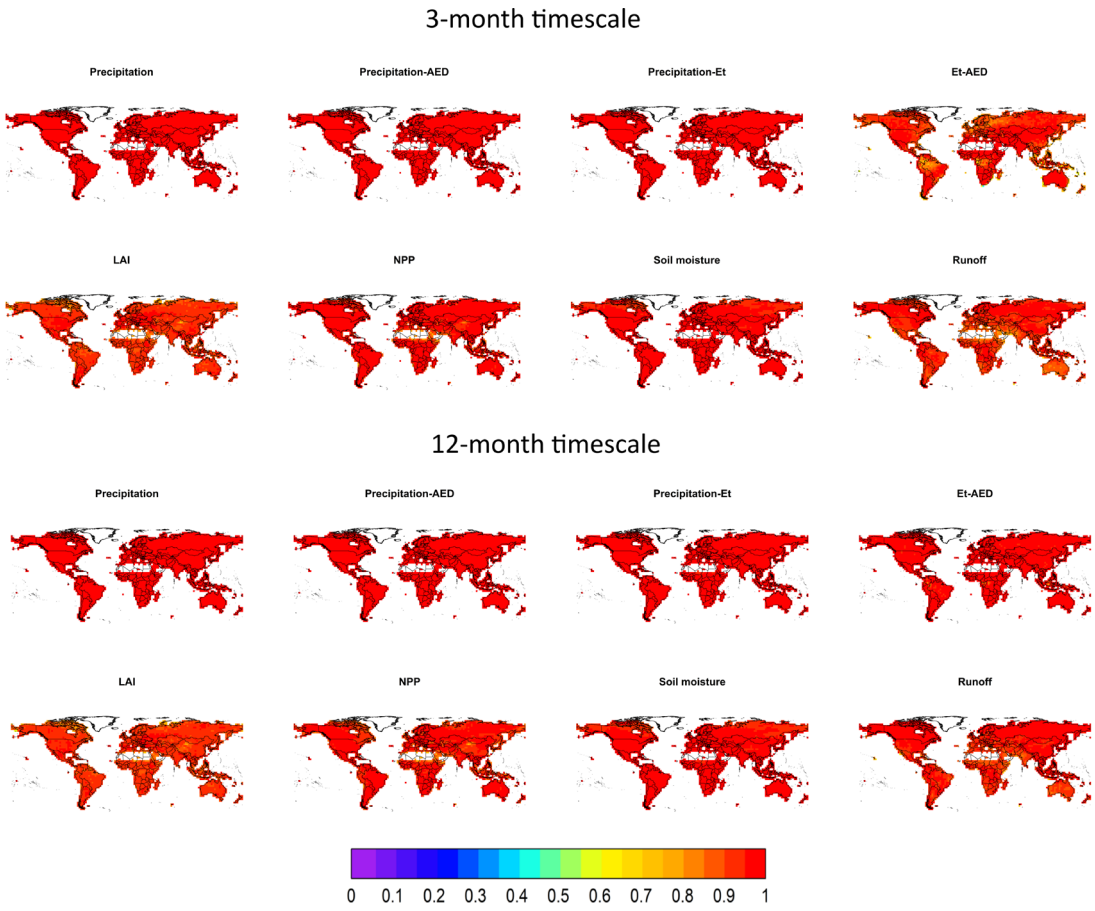

Fig. S1: Average R^2 of the standard normal QQ-plots used for assessing the fit of the index obtained by standardizing the studied variables by means of the log-logistic distribution (gamma distribution for precipitation)

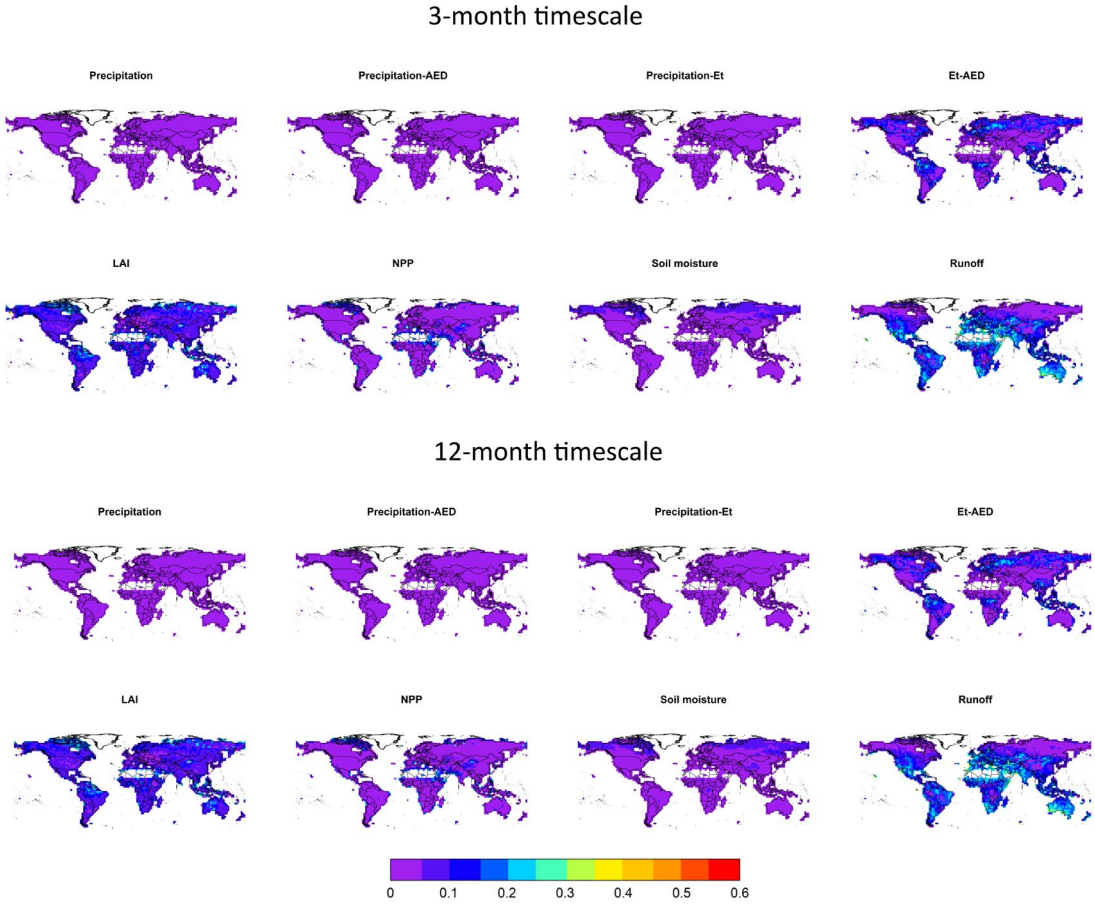

Fig. S2: Standard deviation of the values in Fig. S1

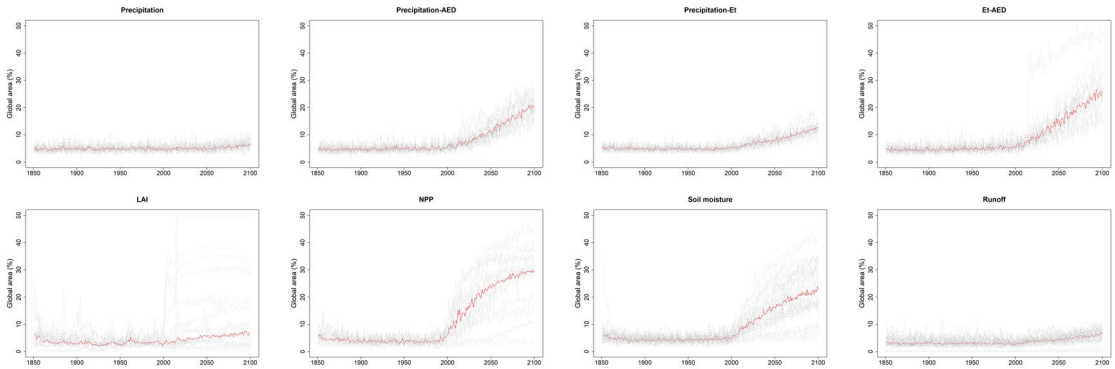

Fig. S3. Average percentage of global land area affected by extreme dry conditions. Same as Fig. 1, but for the evolution of the Boreal winter season (DJF).

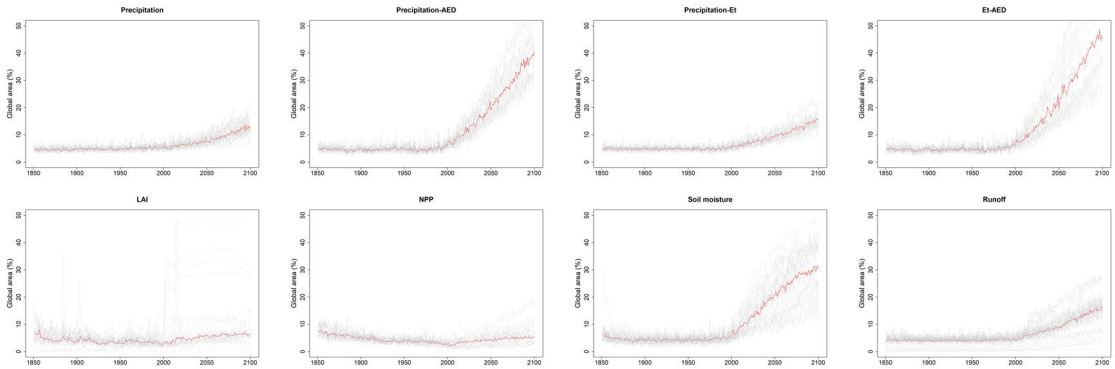

Fig. S4. Average percentage of global land area affected by extreme dry conditions. Same as Fig. 1, but for the evolution of the Boreal summer season (JJA).

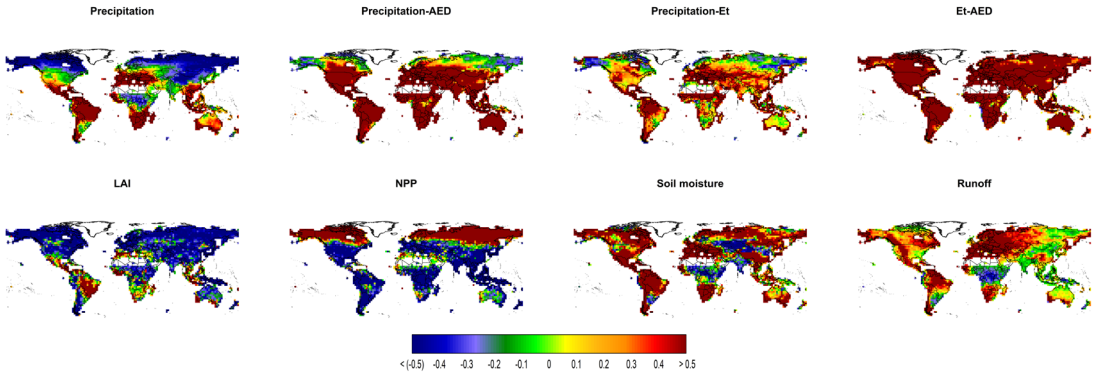

Fig. S5. Spatial distribution of the median trend in the duration of drought events between 1850 and 2100 (Factor: 100).

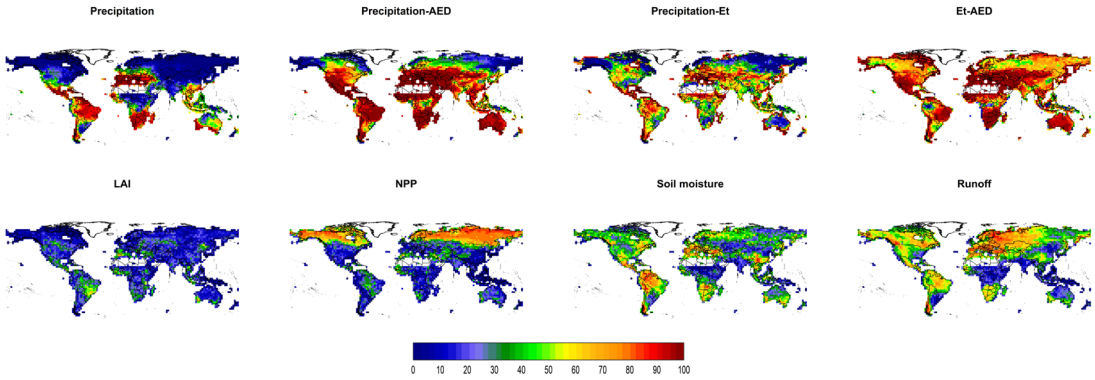

Fig. S6. Percentage of models showing positive and statistically significant trends in drought duration from 1850 to 2100

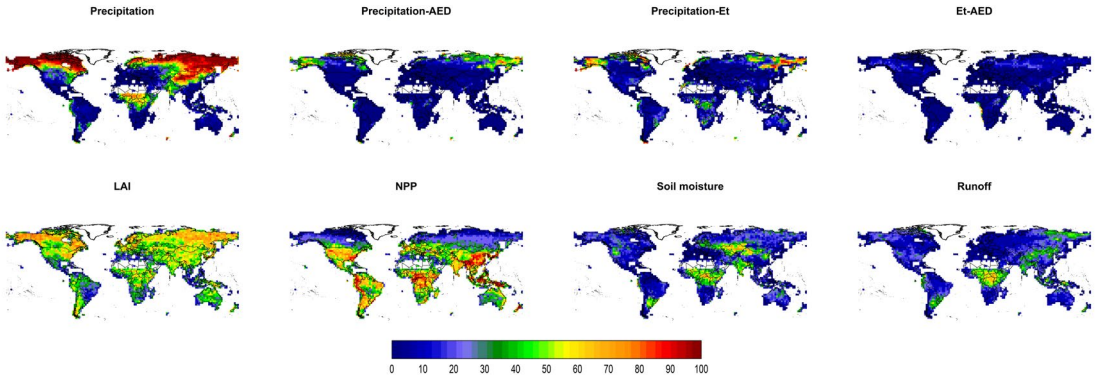

Fig. S7. Percentage of models showing negative and statistically significant trends in drought duration from 1850 to 2100.

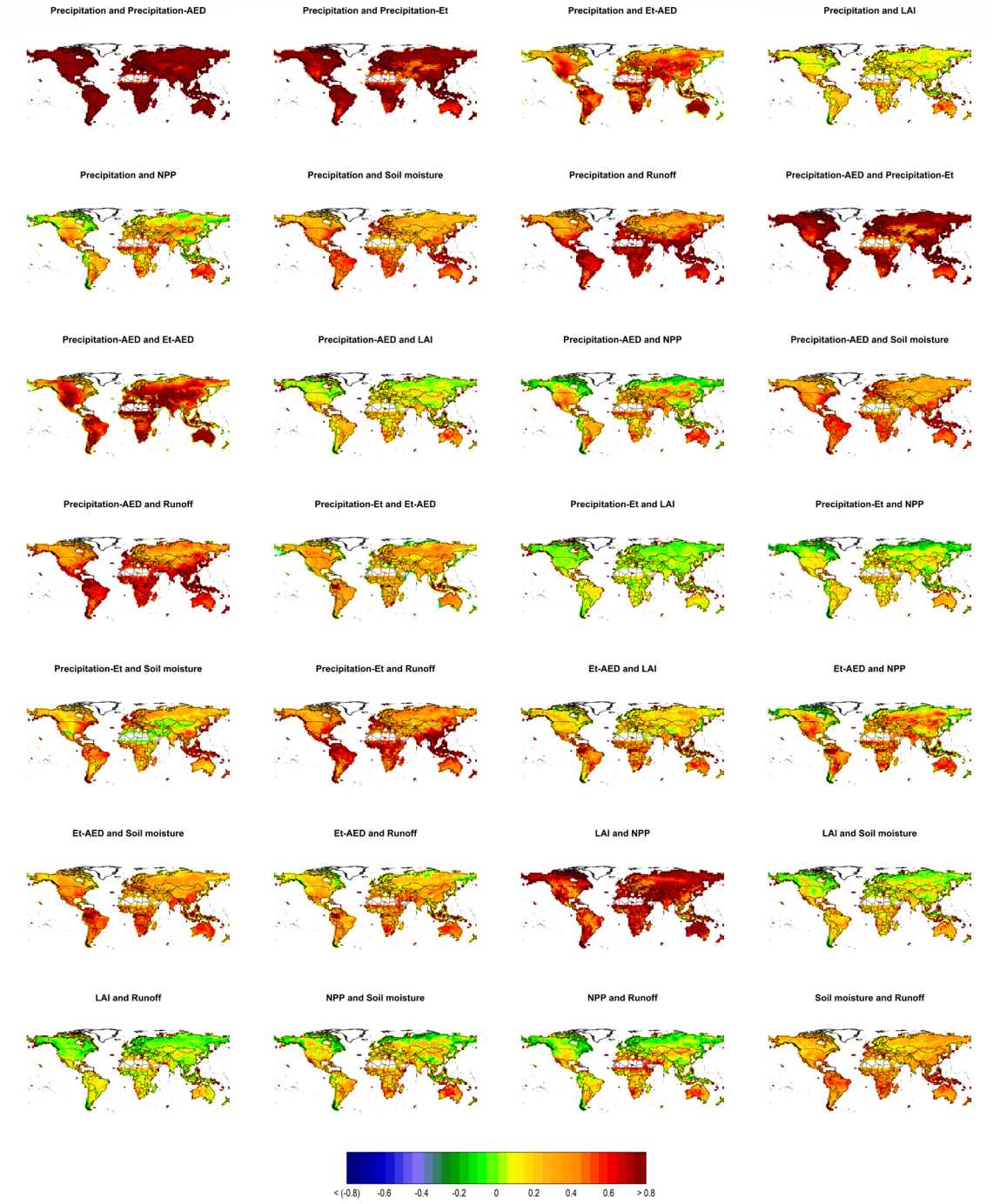

Fig. S8. Median Kendall's τ correlation in the historical period (1850-2014) among the various metrics for the different models

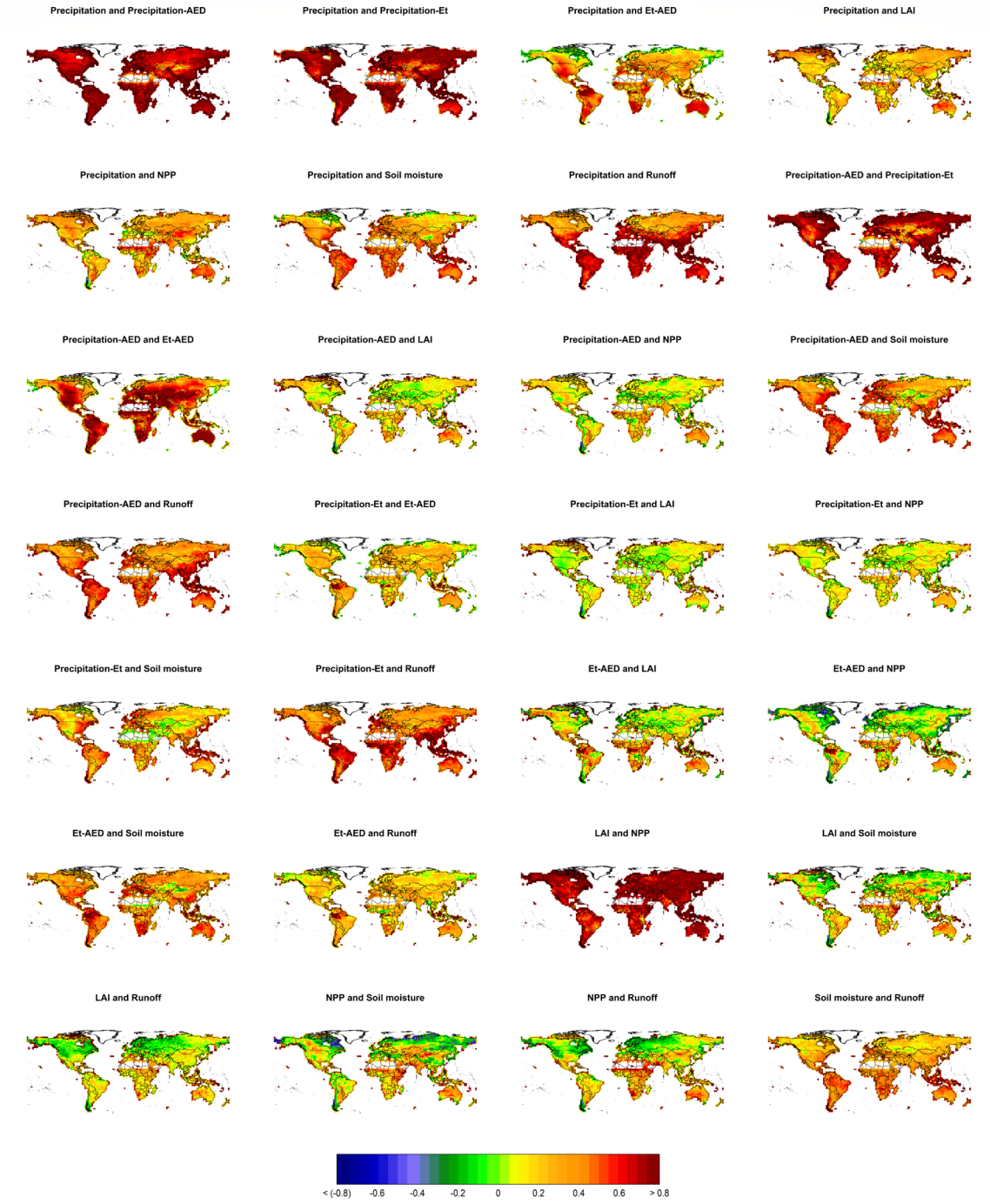

Fig. S9. Median Kendall's τcorrelation in the projected period (2015-2100) among the various metrics for the different models.

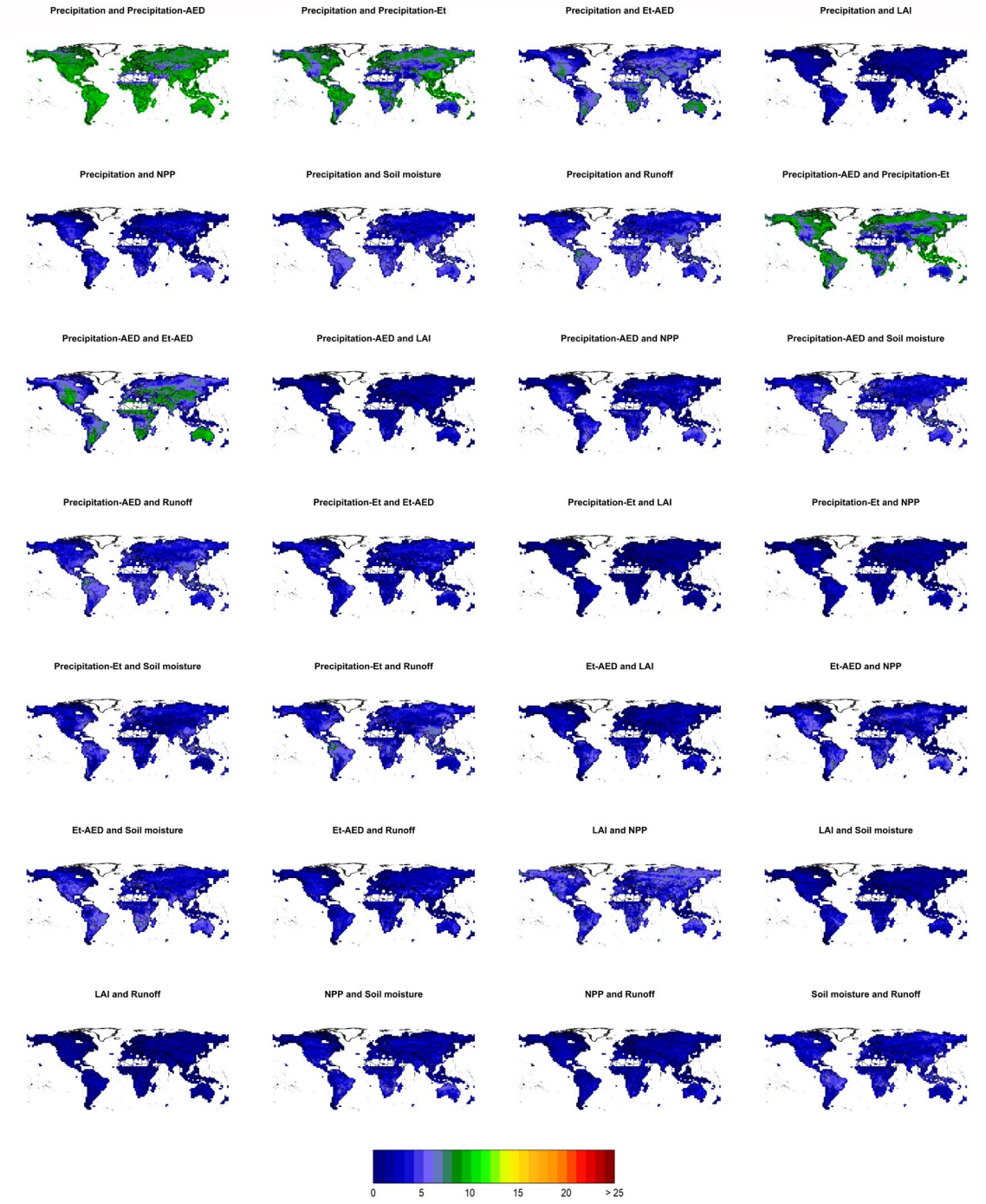

Fig. S10. Average percentage of temporal agreement among the various metrics in the historical period (1850-2014) for the different models.

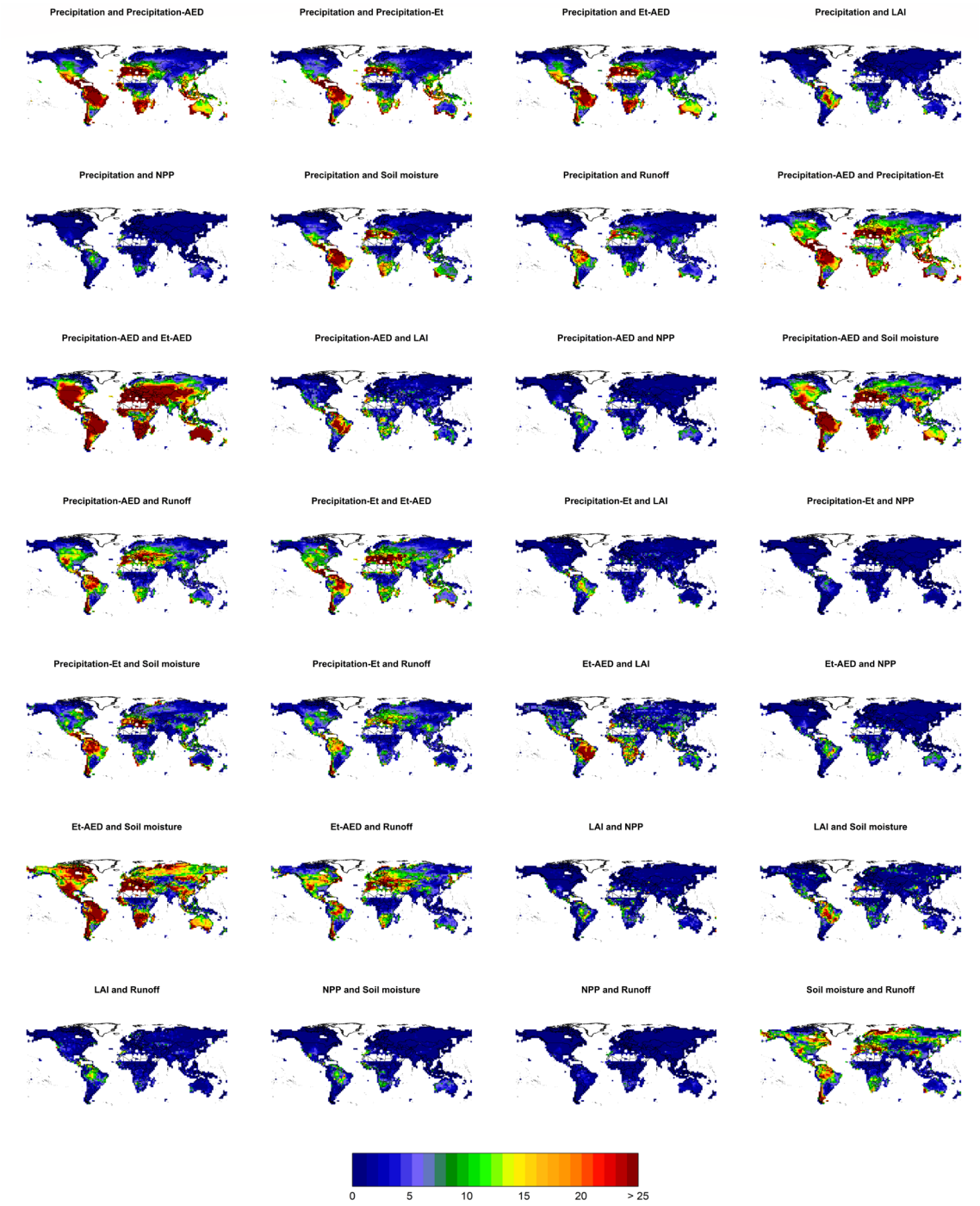

Fig. S11. Average percentage of temporal agreement among the various metrics in the projected period (2015-2100) for the different models.